Pergamon

Int. J. Heat Mass Transfer. Vol. 37, No. 14, pp. 2059–2068, 1994

0017–9310/94 $7.00 + 0.00

0017–9310(94)E0069–7

Transient analysis of thermo-fluid phenomena in twin-roll continuous casting

MAN YEONG HA,† KUISOON KIM,‡ KYUNG CHUN KIM† and SUNG WOO LEE§

†Department of Mechanical and Production Engineering, Pusan National University, Kumjung Ku, Pusan 609-735, Korea

‡Department of Aerospace Engineering, Pusan National University, Kumjung Ku, Pusan 609-735, Korea

§Research Institute of Machinery and Electronics, Samsung Heavy Industries Co., 69 Sinchon-Dong, Changwon, Kyungnam 641-370, Korea

(*Received* 20 *September* 1993 *and in final form* 25 *January* 1994)

Abstract—A computer programme has been developed for analyzing the two-dimensional, unsteady conservation equations for transport phenomena in the molten region of twin-roll continuous casting in order to describe the velocity, and temperature fields, and the solidification process of the molten steel. The energy equation of the cooling roll is solved simultaneously with the conservation equations of molten steel in order to consider heat transfer through the cooling roll. The governing equations are expressed in the generalized coordinates to consider the characteristics of a rotating bank between twin-rollers. In the molten region, it is predicted that transient recirculating flows with small and large vortices are located in the vicinity of the middle of the twin-rollers. The temperature field is affected by the flow fields, showing the complete two-dimensional pattern. The solidification pattern in the molten steel and the temperature distribution in the cooling roll are also obtained as a function of time.

INTRODUCTION

IN RECENT years there has been growing interest in the new continuous casting technologies owing to heavy competition in the steelmaking industries. Twin-roll continuous casting is a promising candidate which has many advantages, such as attractive mechanical properties of rapidly quenched metals or alloys due to their microcrystalline or at times even amorphous structure. In twin-roll continuous casting, molten metal is supplied through a submerged entry nozzle into the rotating bank of two rolls, which rotate in opposite directions. The melt in contact with the roll is cooled down by conduction through the cooling roll, forming a solidified shell which, in proper operation, exits the twin-roll system in the form of a solidified sheet or foil [1, 2].

As solidification proceeds in twin-roll continuous casting, three regions exist; a full solid region, a mushy region (solid plus liquid), and a full liquid region. The modelling of the thermo-fluid characteristics of molten metal for a phase change system is difficult because of the presence of multiple phase, as well as the release of latent heat at the unknown solid–liquid interface. The mathematical and numerical models for mutiphase change with moving interfaces are divided into multiple region and single region formulations.

In the multiple region method, separate conservation equations for each phase are solved, using the appropriate boundary conditions at the interfaces [3–5]. The major difficulty in the multiple region method is the determination of the phase interface as a function of space and time, requiring a moving grid system and/or coordinate transformation procedures. The single region (continuum) formulation is developed from the volume averaging technique based on classical mixture theory and a fixed grid system is employed in the numerical computation of a single set of conservation equations [6–10]. Although this method avoids tracking the phase interface it is difficult to update the release of latent heat at the phase interface, which affects the convergence behaviour of the numerical solution. Voller and co-workers [9–12] at the University of Minnesota suggested methods to accelerate the convergence rate of numerical solution in the fixed grid system by updating the latent heat appropriately from iteration to iteration. Chiang and Tsai [13, 14] considered shrinkage effects in order to calculate the fluid flow and domain change caused by the shrinkage using the single region formulation. Their results were compared with those without shrinkage effects. The results using the single and multiple region methods are compared by Lacroix and Voller [15] with the advantages and disadvantages of each method highlighted.

In the present study, the conservation equations in the molten region are modeled using the single region method which employs a single set of conservation equations for the solid phase, mushy zone, and liquid phase in order to investigate the thermo-fluid phenomena in continuous twin-roll casting. The energy conservation equation of the cooling roll is coupled to the

NOMENCLATURE

c	specific heat [J kg^{-1} K^{-1}]
f	mass fraction
g	volume fraction
h	heat transfer coefficient [W m^{-2} K^{-1}]
H	enthalpy [J kg^{-1}]
J	Jacobian transformation
k	thermal conductivity [W m^{-1} K^{-1}]
K	permeability
L	latent heat [J kg^{-1}]
$L(y)$	distance between the centerline of molten steel and cooling roll surface [m]
P	pressure [N m^{-2}]
r	radial coordinate [m]
S_ϕ	source term for general variable ϕ
t	time [s]
T	temperature [K]
u	x-directional velocity [m s^{-1}]
v	y-directional velocity [m s^{-1}]
x	x-directional coordinate defined in the physical space [m]
y	y-directional coordinate defined in the physical space [m].

Greek symbols

Γ_ϕ	diffusivity for general variable ϕ
ε	emissivity
η	η-directional coordinate defined in the computational space
μ	viscosity [kg s^{-1} m^{-1}]
ξ	ξ-directional coordinate defined in the computational space
ρ	density [kg m^{-3}]
σ	Stefan–Boltzman constant [5.670×10^{-8} W m^{-2} K^{-4}]
ϕ	general variable
φ	circumferential coordinate
ω	angular velocity [rad s^{-1}].

Subscripts

conv	convection
cont	contact
exit	exit
inlet	inlet
l	liquid
ms	molten steel
noz	nozzle
r	roll
rad	radiation
ref	reference
s	solid.

conservation equations in the molten region through the contact boundary. The flow fields, temperature distribution, and solidification pattern in the molten region are obtained as a function of time. The temperature distribution in the cooling roll is also predicted as a function of time. We also considered the effects of roll thermophysical property variation on the time for the system to reach steady state.

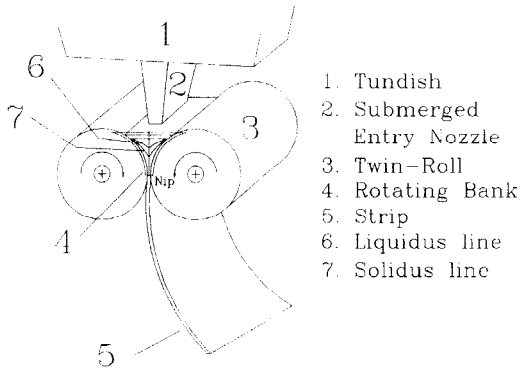

FIG. 1. Schematic diagram of a twin-roll strip casting process.

MATHEMATICAL MODEL

Governing equations

The geometry of a continuous twin-roll casting system is shown in Fig. 1. In order to analyze the fluid flow, temperature fields, and the solidification profiles in the molten steel, this model employed a system of governing equations similar to those developed by Bennon and Incropera [6, 7]. The following assumptions are added to the assumptions made by Bennon and Incropera [6, 7]:

(1) Because molten steel is being supplied with high velocity through a submerged entry nozzle into the nip of two rolls rotating in opposite directions, the flow field is dominated by forced convection and natural convection induced by temperature and composition gradient may be neglected.

(2) Because solidification is completed rapidly in a continuous twin-roll casting, mass transfer due to composition differences is neglected.

In order to consider the characteristics of the rotating bank between the twin-rollers, as shown in Fig. 1, the two-dimensional, unsteady conservation equations for mass, momentum and energy transport in

the molten region are defined in generalized coordinates as follows:

$$\frac{\partial}{\partial t}\left[\frac{1}{J}(\rho\phi)\right]-\frac{\partial}{\partial\xi}\left[\frac{1}{J}\left(\rho G_\xi-\Gamma_\phi g_{11}\frac{\partial\phi}{\partial\xi}\right)\right]-\frac{\partial}{\partial\eta}\left[\frac{1}{J}\left(\rho G_\eta-\Gamma_\phi g_{22}\frac{\partial\phi}{\partial_\eta}\right)\right]=\frac{\partial}{\partial\xi}\left[\frac{1}{J}\left(\Gamma_\phi g_{12}\frac{\partial\phi}{\partial\eta}\right)\right]+\frac{\partial}{\partial\eta}\left[\frac{1}{J}\left(\Gamma_\phi g_{12}\frac{\partial\phi}{\partial\xi}\right)\right]+\frac{S_\phi}{J} \quad (1)$$

where

$$G_\xi = u\frac{\partial\xi}{\partial x}+v\frac{\partial\xi}{\partial y} \quad (2)$$

$$G_\eta = u\frac{\partial\eta}{\partial x}+v\frac{\partial\eta}{\partial y} \quad (3)$$

$$g_{11} = \left(\frac{\partial\xi}{\partial x}\right)^2+\left(\frac{\partial\xi}{\partial y}\right)^2 \quad (4)$$

$$g_{22} = \left(\frac{\partial\eta}{\partial x}\right)^2+\left(\frac{\partial\eta}{\partial y}\right)^2 \quad (5)$$

$$g_{12} = \left(\frac{\partial\xi}{\partial x}\right)\left(\frac{\partial\eta}{\partial x}\right)+\left(\frac{\partial\xi}{\partial y}\right)\left(\frac{\partial\eta}{\partial y}\right). \quad (6)$$

In the conservation of momentum equation, $\phi = u, v$ represent the mixture velocities in the x and y directions, respectively, defined as

$$\phi = f_s\phi_s+f_l\phi_l \quad (\phi = u, v) \quad (7)$$

where f is the mass fraction of the mixture. The subscripts s and l represent the solid and liquid phase, respectively. In the energy equation H is the mixture enthalpy defined as

$$H = (f_s c_s+f_l c_l)T+\Delta H \quad (8)$$

where

$$\Delta H = \begin{cases} L, & T \geqslant T_l \\ L(1-f_s), & T_s < T < T_l \\ 0, & T \leqslant T_s \end{cases} \quad (9)$$

where L is a latent heat and T_l and T_s represent the liquids and solidus temperature, respectively. In the present study, the simple linear form for the local solid mass fraction f_s and temperature relationship is used

$$f_s = \begin{cases} 0, & T \geqslant T_l \\ \dfrac{T_l-T}{T_l-T_s}, & T_s < T < T_l \\ 1, & T \leqslant T_s \end{cases} \quad (10)$$

Similarly, the mixture density and thermal conductivity are

$$\rho = g_s\rho_s+g_l\rho_l \quad k = g_s k_s+g_l k_l \quad (11)$$

where g is the volume fraction. The source terms $S\phi$ in equation (1) are given in Table 1. The permeability K in Table 1 makes the x- and y-momentum equations reduce to the appropriate single phase limits as $K \to 0$ (pure solid) and $K \to \infty$ (pure liquid). In the present investigation, the following formula for K taken by Bennon and Incropera [6,7] is used:

$$K = K_0\frac{g_l^3}{(1-g_l)^2}. \quad (12)$$

The u_s and v_s in the momentum equation of Table 1 is the velocity of the solid phase prescribed by the rotating roll, defined as

$$u_s = (y-y_0)\omega, \quad v_s = -(x-x_0)\omega \quad (13)$$

where ω is the angular speed of the rotating roll.

In order to investigate the heat transfer in the rotating roll, the following two-dimensional, unsteady equation for conductive heat transfer is solved in the coordinate system fixed in the rotating roll:

$$\rho_r c_r\frac{\partial T}{\partial t} = \frac{1}{r}\frac{\partial}{\partial r}\left(k_r r\frac{\partial T}{\partial r}\right)+\frac{1}{r}\frac{\partial}{\partial\varphi}\left(\frac{k_r}{r}\frac{\partial T}{\partial\varphi}\right). \quad (14)$$

ρ_r, c_r and k_r represent the density, specific heat and thermal conducivity, respectively, which depend on the temperature field. In the present calculations, two different materials are selected to consider the effects of material property variation on the cooling capacity of roll. The thermophysical properties for the first cooling roll (Type I) as a function of temperature are expressed as

$$\rho_r = 7811.206-0.20517T-0.000068T^2 \quad (15)$$

$$c_r = 488.392+0.2091T+0.000096T^2 \quad (16)$$

$$k_r = 42.69+0.01016T-0.000028T^2. \quad (17)$$

Similarly the thermophysical properties for the second cooling roll (Type II) are

$$\rho_r = 9026.8906-0.40802T-0.0001T^2 \quad (18)$$

$$c_r = 379.2776+0.019659T+0.000597T^2 \quad (19)$$

$$k_r = 311.2472+0.07211T-0.0000001T^2. \quad (20)$$

The major differences in the thermophysical properties of roll Type I and II are the thermal conductivity.

Table 1. Source terms S_ϕ used in equation (1)

ϕ	Γ_ϕ	$\frac{S_\phi}{J}$
1	0	0
u	$\mu\frac{\rho}{\rho_l}$	$-\left(\frac{\xi_x}{J}\right)\frac{\partial p}{\partial\xi}-\left(\frac{\eta_x}{J}\right)\frac{\partial p}{\partial\eta}-\left(\frac{\mu_l}{K}\right)\left(\frac{\rho}{\rho_l}\right)(u-u_s)$
v	$\mu\frac{\rho}{\rho_l}$	$-\left(\frac{\xi_y}{J}\right)\frac{\partial p}{\partial\xi}-\left(\frac{\eta_y}{J}\right)\frac{\partial p}{\partial\eta}-\left(\frac{\mu_l}{K}\right)\left(\frac{\rho}{\rho_l}\right)(v-v_s)$
h	$\frac{k}{c_s}$	$\nabla\left[\frac{k}{c_s}\nabla(h_s-h)\right]-\nabla[\rho(h_l-h)(\mathbf{V}-\mathbf{V}_s)]$

The thermal conductivity of Type II is higher than that of Type I.

Initial and boundary conditions

The conservation equations (1) and (14) govern the thermo-fluid phenomena in the molten steel and the temperature distribution in the cooling roll, respectively. They are unsteady and elliptic partial differential equations, requiring initial and boundary conditions. We used $u = v = 0$ as initial velocities in the molten region, and the temperature of the molten steel supplied through the nozzle as the initial temperature. The ambient room temperature is used as the initial temperature of the cooling roll.

The following boundary conditions in the molten region are used in the coordinate system shown in Fig. 2:

Symmetry (x = 0),

$$\frac{\partial \phi}{\partial x} = 0. \tag{21}$$

Exit ($y = H_{pool}$),

$$u = 0, \quad v = v_{exit}, \quad \frac{\partial T}{\partial x} = 0. \tag{22}$$

Nozzle,

$$u = 0, \quad v = v_{inlet}, \quad T = T_{inlet},$$
$$\text{at} \quad y = y_{noz} \quad \text{and} \quad 0 < x < x_{noz} \tag{23}$$

$$u = v = 0, \quad T = T_{inlet},$$
$$\text{at} \quad y = y_{noz} \quad \text{and} \quad x_{noz} < x < x_l(y) \tag{24}$$

$$u = v = 0, \quad T = T_{inlet},$$
$$\text{at} \quad x = x_l \quad \text{and} \quad 0 < y < y_{noz}. \tag{25}$$

Pool surface, y = 0 *and* $x_l < x < L_0$,

$$\frac{\partial u}{\partial y} = 0, \quad v = 0, \quad T = T_{inlet}. \tag{26}$$

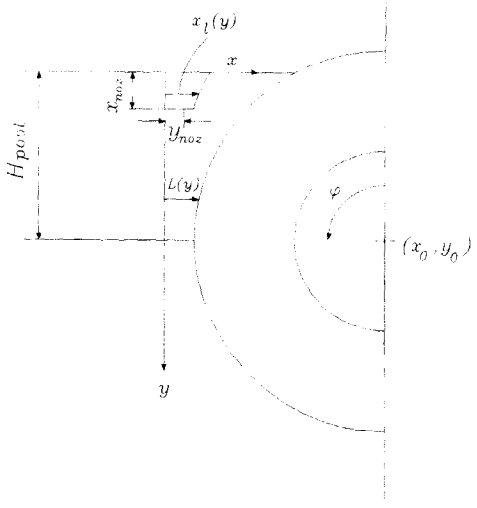

FIG. 2. Coordinate system used in the present calculation.

Contact region between the molten steel and cooling roll, x = L(y),

$$u = (y - y_0)\omega, \quad v = -(x - x_0)\omega,$$
$$-k\frac{\partial T}{\partial n} = h_{cont}(T - T_{roll}). \tag{27}$$

v_{exit} in equation (22) is the exit velocity of the molten steel specified from the operating conditions, and v_{inlet} in equation (23) represents the inlet velocity obtained from mass conservation and v_{inlet}. T_{inlet} is the temperature of the molten steel supplied through the nozzle. The no slip condition is used for the velocity boundary condition of the contact region (see equation (26)). ω is the angular speed of the cooling roll. x_0 and y_0 are the coordinates of the center of the cooling roll. h_{cont} in equation (26) is the contact heat transfer coefficient between the molten steel and the cooling roll and the calculated results are influenced by the choice of h_{cont} value. T_{roll} is the surface temperature of the cooling roll at the contact region.

For the boundary conditions in the circumferential direction φ of the cooling roll, we used the perioic boundary conditions which have the same temperature and heat flux at $\varphi = 0$ and 2π. A constant temperature of 20°C is used as a boundary condition at the inner surface of the roll in contact with the cooling water passing through the inner hole at the center of the roll. At the outer surface of the roll which is not in contact with the molten steel, the following convective and radiative cooling conditions are used:

$$-k_s\frac{\partial T}{\partial r} = h_{conv}(T - T_\infty) + h_{rad}(T - T_\infty) \tag{28}$$

where

$$h_{rad} = \sigma\varepsilon(T^2 - T_\infty^2)(T + T_\infty). \tag{29}$$

At the surface of the roll in contact with the molten steel, a similar condition to equation (27) is used:

$$-k\frac{\partial T}{\partial n} = h_{cont}(T_{ms} - T). \tag{30}$$

T_{ms} is the temperature of molten steel in contact with the roll. Thus the molten steel and cooling roll are coupled through heat transfer conditions given by equations (27) and (30) and must be solved simultaneously.

The numerical solution of the conservation equations for molten steel and cooling roll is obtained using the finite difference method. A non-staggered grid is adopted for the numerical solution of the momentum equation of molten steel. Using an explicit Euler scheme [16], the numerical solution of the energy equation (14) in the cooling roll is obtained. The heat transfer rate in the contact region between the molten steel and cooling roll is calculated from equation (27). Using this heat flux and specified boundary conditions, the solutions of conservation equation (1) for molten steel are obtained using the SIMPLE/PWIM of Rhie and Chow [17], calculating

the heat flux from the molten steel to the roll. This procedure is repeated with increased time step until it reaches the specified time limit.

RESULTS AND DISCUSSION

In order to check the accuracy of the model, we first simulated the solidification process in the thermal cavity which employs the same configuration used by Voller and Prakash [9]. The temperature of one vertical surface of the thermal cavity is fixed at a value below the freezing temperature while maintaining the opposing surface above the freezing temperature. The top and bottom surfaces are insulated. Figure 3 shows the shape of the mushy region bounded by the solidus and liquidus line, represented in Fig. 3 by 0.1 and -0.1. The left-hand figure in Fig. 3 represents the results obtained from the present numerical solution whereas the right-hand figure represents those of Voller and Prakash [9]. We also compared the velocity vectors and isothermal lines. The results from the present numerical solutions compare well with those of Voller and Prakash [9] for the solidification process in the thermal cavity under the same number of grid, time step and input data.

After the successful benchmarks made with the solidification in the thermal cavity, the program was run for the case of thermo-fluid dynamics in a continuous casting. The material selected was steel (SUS 304) with the principal data shown in Table 2. Figure 4 shows the grid system used in the molten steel, locating more grids close to the roll considering the high gradients. A sensitivity analysis was carried out in order to check the dependence of the calculated results on the number of grids. The number of grids used is 40 in the x and 91 in the y direction, considering the accuracy and computational time.

Figures 5 and 6 show the velocity vectors and streamlines, respectively, after 2, 6 and 10 revolutions of the rotating roll. The angular speed of roll is $\omega = 0.822\ \text{rad s}^{-1}$ ($v_{\text{exit}} = 18.5\ \text{m s}^{-1}$) and the roll used

Table 2. Principal data and parameters in the present calculation

Specific heat [J kg^{-1}K^{-1}]	681.45
Thermal conductivity [W m^{-1}K^{-1}]	29.9
Density [kg m^{-3}]	7340.1
Viscosity [kg ms^{-1}]	4.4×10^{-4}
Latent heat [J kg^{-1}]	2.6×10^{5}
Liquidus temperature [K]	1724
Solidus temperature [K]	1672
Initial temperature [K]	1773
Roll diameter [m]	0.625
Height of pool surface [m]	0.5
Angle between pool surface and roll outlet [degrees]	53.13
K_0	1.6×10^{7}
x_{nozz} [m]	0.0035
y_{nozz} [m]	0.034
x_0 [m]	0.3766
y_0 [m]	0.215
h_{conv} [W m^{-2} K]	19.5
ε	1.0
T_∞ [K]	293

is Type I whose properties are given in equations (15)–(17). The molten steel supplied through the nozzle has high velocity with small area at the exit. Because the area at the nozzle exit increases abruptly, the molten steel is expanded and directed to the rotating roll with decreasing velocity. The molten steel close to the rotating roll changes its direction due to the rotating roll and moves to the nip point. Upstream close to the nozzle, a large vortex is formed with small vortices inside the large vortex. A small closed vortex is also observed around the nozzle. The solid phase close to the roll moves to the nip with a velocity of $r\omega$ given in equation (13), where r is the distance from the center of the roll. Miyazawa and Szekely [1] and Saitoh *et al.* [2] solve parabolic momentum equations, assuming that momentum transfers occus mainly along the centerline direction. However, as shown in Fig. 6, recirculating flow exists in the molten region, meaning that

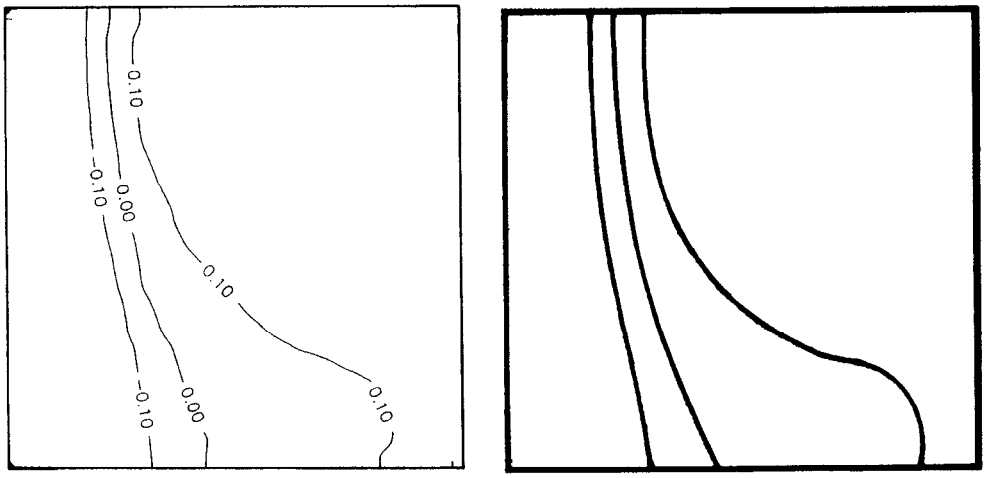

FIG. 3. Solidus and liquidus lines in the thermal cavity.

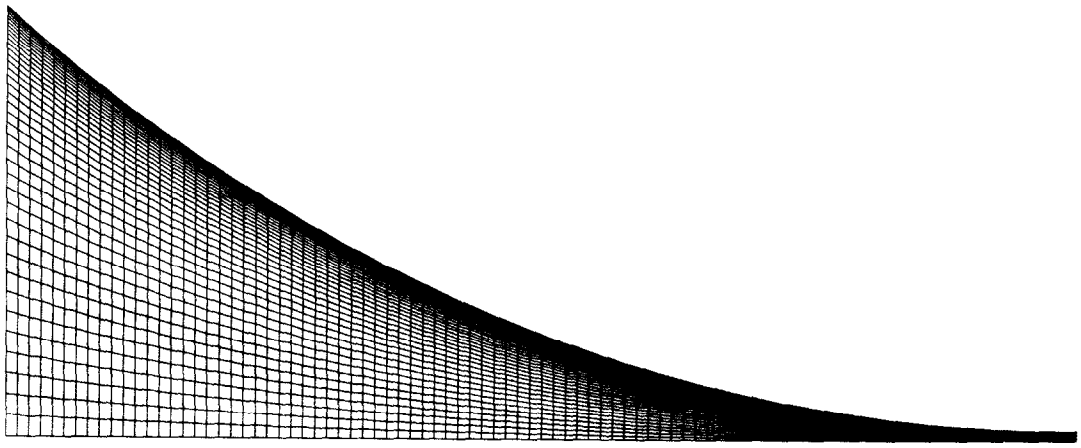

FIG. 4. Grid used in the molten steel.

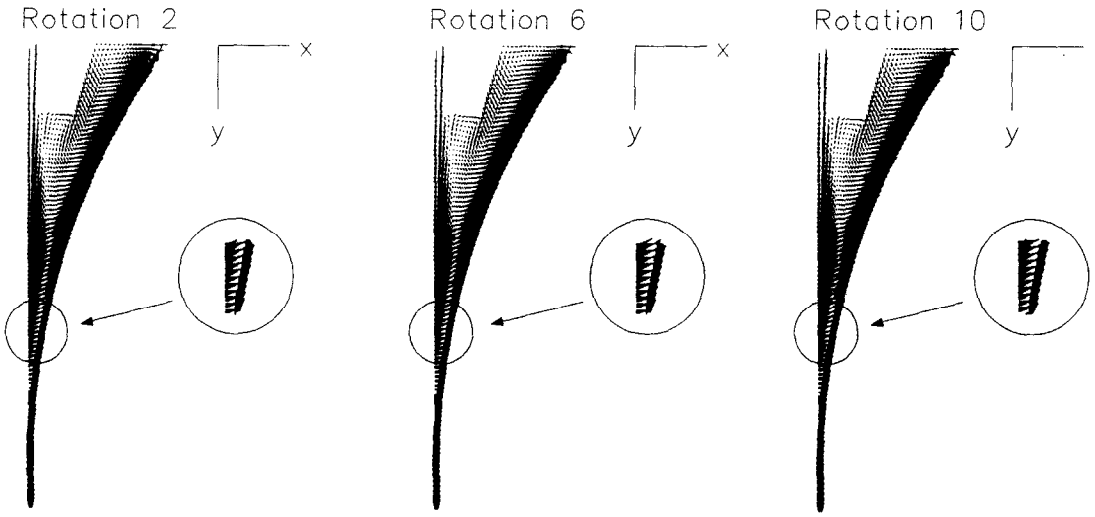

FIG. 5. Velocity vector in the molten steel as a function of revolution of the roll; roll Type I.

the flow fields should be obtained through the full elliptic Navier–Stokes equations.

Figure 7 shows the solidus and liquidus lines after 2, 6 and 10 revolutions of the rotating roll. An isothermal line of $T = 1672$ K corresponds to the solidus line which is located in the vicinity of the roll surface. An isothermal line of $T = 1724$ K is defined as the liquidus line. The solid and liquid phase coexist in the mushy region which is distributed at the very narrow range between the solidus and liquidus line in the case of rapid solidification of twin-roll casting. Most of the rotating bank is in the liquid phase. Figure 8 shows the isothermal lines after two, six and ten revolutions. Downstream close to the nip, the thickness is very small compared to the upstream close to the nozzle and the interval of the isothermal lines is very narrow, showing one-dimensional profiles. However, upstream close to the nozzle, the interval of isothermal lines increases and the temperature fields are affected by the recirculating flows shown in Figs. 5 and 6, and exhibit two-dimensional profiles. These results show that the solidification pattern and temperature fields in the molten region are affected by the flow fields, requiring the simultaneous solution of elliptic conservation equations of mass, momentum and energy.

Figure 9 shows the temperature distribution in the cooling roll after five and ten revolutions. The isothermal lines extend from 350 K and continue to 800 K, with intervals of 50 K. Temperatures greater than 800 K are distributed closer to the roll surface and are not shown in Fig. 9. The temperature at the roll surface is high with the repeated heating and cooling while the roll is in contact with the molten region and the atmosphere. Moving from the roll surface to the center, the temperature decreases with the cooling due to heat transfer to the cooling water passing through the hole at the center of the roll. Close to the roll surface, the temperature gradient is high, giving the large thermal stress. Figure 10 shows the temperature at an arbitrary location of the roll as a function of time. The temperature shows maximum when the roll

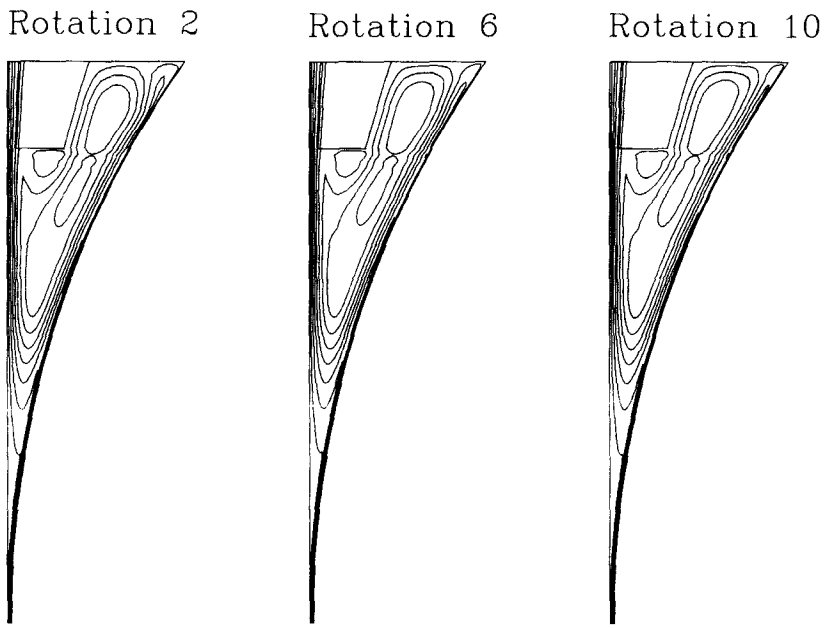

FIG. 6. Stream function in the molten steel as a function of revolution of the roll; roll Type I.

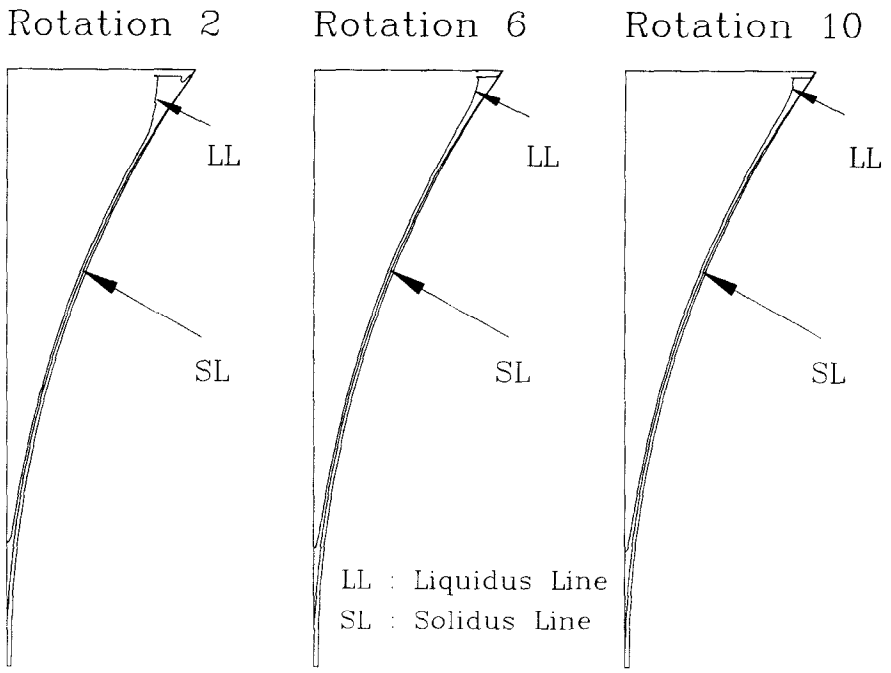

FIG. 7. Solidus and liquidus lines in the molten steel as a function of revolution of the roll; roll Type I.

is in contact with the molten steel and decreases due to the cooling due to the heat transfer to the cooling water. The maximum and minimum temperatures after ten revolutions are about 1140 K and 660 K, respectively. Because the cooling capacity of roll is not sufficiently high, the roll does not reach a complete steady state, and the maximum and minimum temperatures increase slowly.

In order to consider the effects of the material property variation on the solidification, the roll of Type II with thermophysical properties given by equations (18)–(20) is used. The global characteristics of flow, temperature and solidification distribution in the molten region using Type I are similar to the case using the roll of Type II. Figure 11 shows the temperature at a specified location of roll as a function of time for $\omega = 0.822$ rad s^{-1} ($v_{exit} = 18.5$ m s^{-1}) using the roll of Type II. After ten revolutions, the maximum and minimum temperature are about 740 K and 540 K, lower than those using the roll of Type I due to the increased cooling capacity with increasing thermal conductivity.

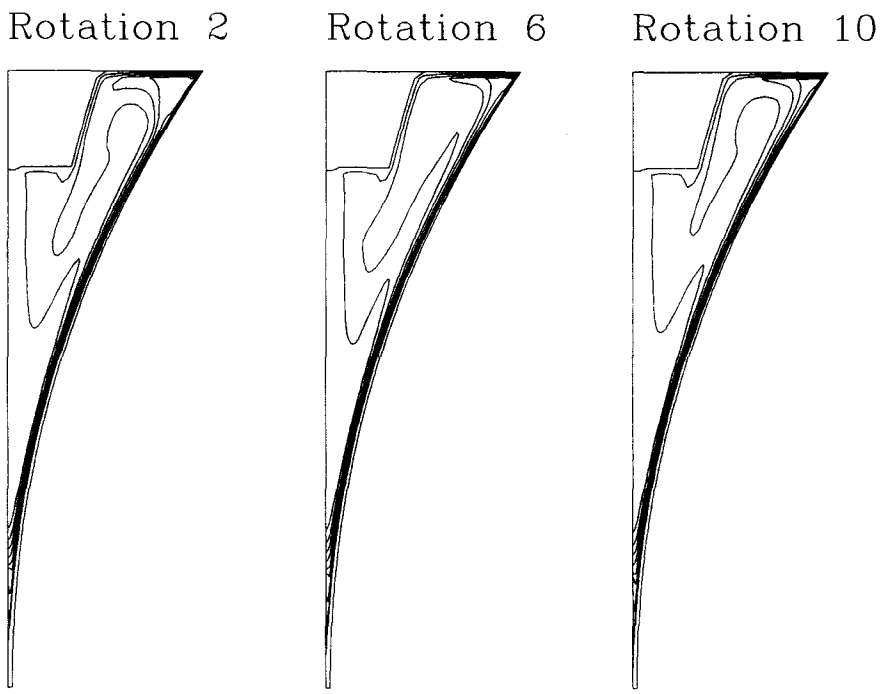

FIG. 8. Isothermal lines in the molten steel as a function of revolution of the roll; roll Type I.

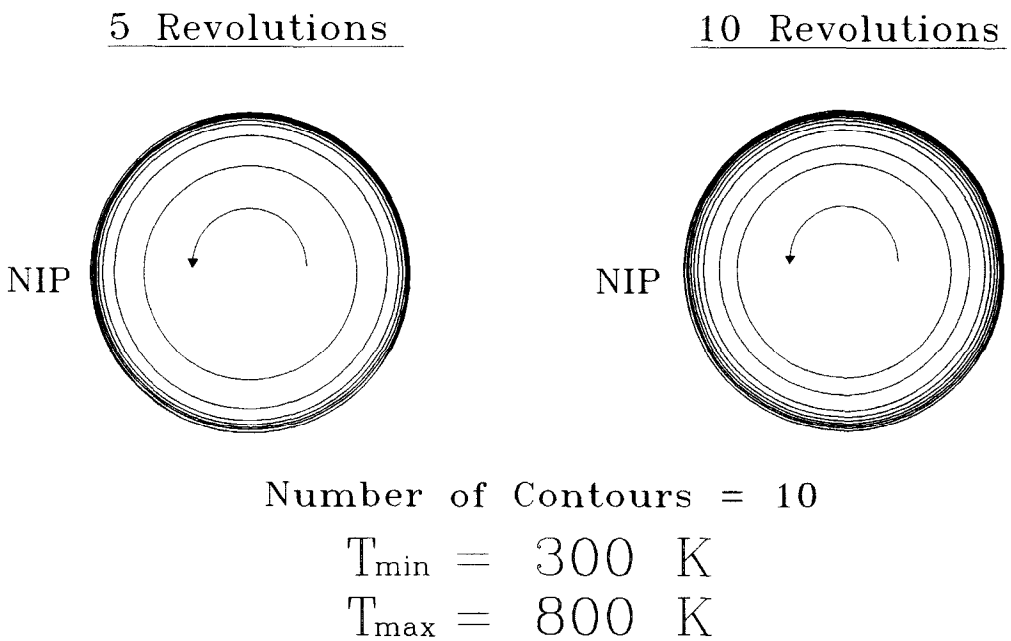

FIG. 9. Isothermal lines in the cooling roll as a function of revolution of the roll; roll Type I.

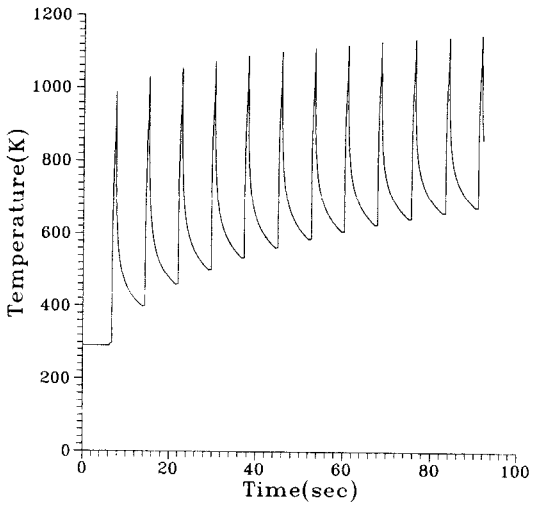

FIG. 10. Temperature at the surface as a function of time; roll Type I.

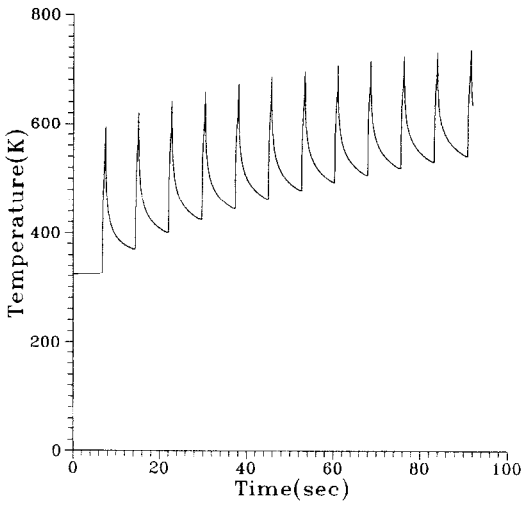

FIG. 11. Temperature at the surface as a function of time; roll Type II.

One of the most important operating conditions in the twin-roll continuous casting is a location where the solidification is completed. If the solidification is not completed at the nip point, the strip exits the system with a liquid phase or mushy region causing bulging phenomena. In the case that the solidification is completed too early, roll separating forces are very large, resulting in large roll deformation. Thus the allowed operating conditions fall in the very narrow range. Figure 12 shows the distance from the nip to the solidification point at the centerline as a function of time for the roll of Type I and II. For roll Type I, the distance from the nip to the solidification point increases at the initial period of cooling reaching a maximum value around 10 s. Since the cooling capacity of the Type I roll is lower, the temperature in the cooling roll increases and the solidification point moves to the nip point during the subsequent cooling period. The distance after ten revolutions is about 4 mm. This result shows that the system does not reach steady state using $\omega = 0.822$ rad s^{-1} and Type I cooling roll. However, due to the increased cooling ability with increasing thermal conductivity, the roll of Type II under the same operating condition reaches steady state and the distance from the nip to the solidification point is about 26 mm. The strip thickness in the longitudinal direction depends on the temperature distribution in that direction. For the roll of Type I, the roll does not reach steady state and the strip temperature and thickness are not uniform in the longitudinal direction. If the roll of Type II is used, steady state is reached at an early time of cooling, the strip temperature and thickness are uniform, producing the strip satisfying the required specification.

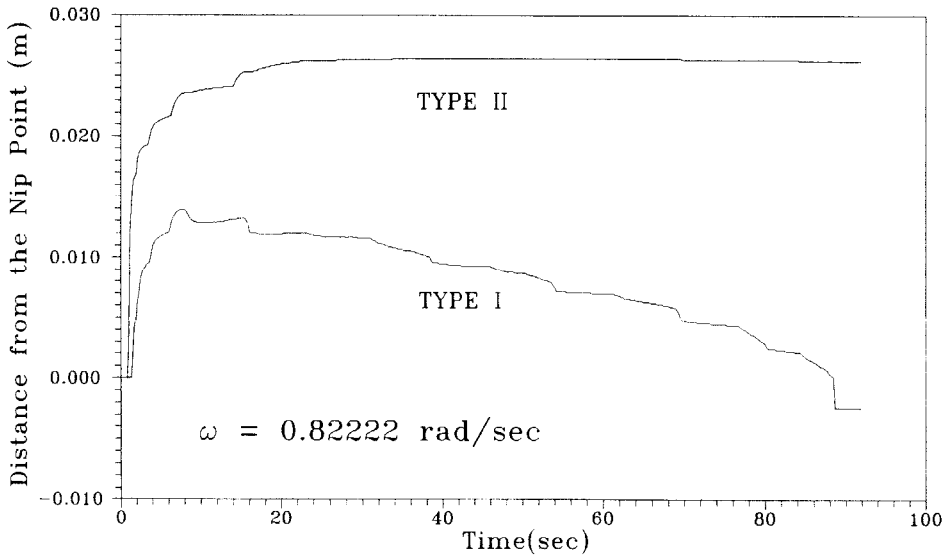

FIG. 12. Solidus point at the centerline of molten steel as a function of time.

SUMMARY AND CONCLUSIONS

(1) We developed a computer code to solve the two-dimensional, unsteady conservation equations for mass, momentum and energy transport in the molten region, and the energy conservation equation in the cooling roll simultaneously.

(2) The temperature distribution in the molten region exhibits two-dimensional profiles affected by the recirculating flow with small and large vortices. As the thermal conductivity of the roll increases, a steady state reaches at an early time, giving lower temperature distribution in the roll and longer distance from the nip to the solidification point than the roll of Type I. The roll of Type I does not reach a steady state after ten revolutions.

(3) From the present calculation, we can determine when the system reaches its steady state. If the process does not reach steady state at an early time, the different temperature distribution in the longitudinal direction will produce a strip with non-uniform thickness, degrading the quality of the product. The flow and temperature distribution in the molten region and the temperature distribution in the roll can be used to determine the roll separating force and thermal stress and deformation (thermal crown) in the width direction of roll, which are important design variables in the design of cooling roll.

Acknowledgement—The financial support of the Samsung Heavy Industries Co. is gratefully acknowledged.

REFERENCES

1. K. Miyazawa and J. Szekely, Mathematical model of the splat cooling process using the twin-roll technique, *Metall. Trans. A* **12A,** 1047–1057 (1981).
2. T. Saitoh, H. Hojo, H. Yaguchi and C. G. Kang, Two-dimensional model for twin-roll continuous casting, *Metall. Trans. B* **20B,** 381 390 (1989).
3. C. F. Hsu, E. M. Sparrow and S. V. Patankar, Numerical solution of moving boundary problems by boundary immobilization and a control-volume-based finite-difference scheme, *Int. J. Heat Mass Transfer* **24,** 1335–1343 (1981).
4. D. Poulikakos and W. Cao, Solidification of a binary alloy from a cold wire or pipe: modeling of the mixed-phase region, *Numer. Heat Transfer* **15,** 197–219 (1989).
5. G. H. Yeoh, M. Behnia, G. De Vahl Davis and E. Leonardi, A numerical study of three-dimensional natural convection during freezing of water, *Int. J. Numer. Meth. Engng* **30,** 899–914 (1990).
6. W. D. Bennon and F. P. Incropera, A continuum model for momentum, heat and species transport in binary solid–liquid phase change systems—I. Model formulation, *Int. J. Heat Mass Transfer* **30,** 2161–2170 (1987).
7. W. D. Bennon and F. P. Incropera, A continuum model for momentum, heat and species transport in binary solid–liquid phase change systems—II. Application to solidification in a rectangular cavity, *Int. J. Heat Mass Transfer* **30,** 2171–2187 (1987).
8. W. D. Bennon and F. P. Incropera, Numerical analysis of binary solid–liquid phase change using a continuum model, *Numer. Heat Transfer* **13,** 277–296 (1988).
9. V. R. Voller and C. Prakash, A fixed grid numerical modelling methodology for convection–diffusion mushy region phase-change problems, *Int. J. Heat Mass Transfer* **30,** 1709–1719 (1987).
10. V. R. Voller, C. R. Swaminathan and B. G. Thomas, Fixed grid techniques for phase change problems: a review, *Int. J. Numer. Meth. Engng* **30,** 875–898 (1990).
11. V. R. Voller, Fast implicit finite-difference method for the analysis of phase change problems, *Numer. Heat Transfer* **17,** 155–169 (1990).
12. C. Prakash and V. R. Voller, On the numerical solution of continuum mixture model equations describing binary solid–liquid phase change, *Numer. Heat Transfer* **17,** 155–169 (1989).
13. K. C. Chiang and H. L. Tsai, Shrinkage-induced fluid flow and domain change in two-dimensional alloy solidification, *Int. J. Heat Mass Transfer* **35,** 1763–1770 (1992).
14. K. C. Chiang and H. L. Tsai, Interaction between shrinkage-induced fluid flow and natural convection during alloy solidification, *Int. J. Heat Mass Transfer* **35,** 1771–1778 (1992).
15. M. Lacroix and V. R. Voller, Finite difference solutions of solidification phase change problems: transformed vs fixed grids, *Numer. Heat Transfer* **17,** 25–41 (1990).
16. J. Thibault, Comparison of nine three-dimensional numerical methods for the solution of the heat diffusion equation, *Numer. Heat Transfer* **8,** 281–288 (1985).
17. C. M. Rhie and W. L. Chow, Numerical study of the turbulent flow past an airfoil with trailing edge separation, *AIAA J.* **21,** 1525–1532 (1983).